CHAPTER -6

LCF Behaviour of Salt Coated and Pre-exposed Inconel 617 Alloy

6.1 Introduction

This chapter deals with low cycle fatigue (LCF) behaviour of the Inconel 617 alloy, after oxidation at 850^{o}C for varying durations, without and with mixed salt coating. LCF tests were conducted under fully reversed axial strain controlled mode at strain rate of $5x10^{-3}$ s^{-1} and strain amplitude of ±0.25% at 850^{o}C to examine the influence of oxidation and mixed salt coating of 10% NaCl+ 90% Na_2SO_4, on fatigue life and deformation behaviour under cyclic loading. During application of Inconel 617 alloy as combustion chamber lining in gas turbine engines, they experience high temperatures and also expose to deleterious salt environment when the aircrafts pass through marine atmospheres. The fused salt deposits of Na_2SO_4 and NaCl attack the surface of the alloy and accelerate the corrosion process (Type I corrosion) at elevated temperatures [70]. NaCl is mainly accrued from the combustion air of the marine environment in the form of tiny particles and its reaction with sulphur from fuel forms Na_2SO_4. In addition, the alloy also experiences thermal stresses and localised plastic strains due to high temperatures during repeated start up and shut down events in these applications. Consideration of LCF data under oxidising and saline environment is therefore of utmost importance while designing components of gas turbine engines and thus forms the basis of the investigation for the present chapter.

Creep-fatigue interaction in hot corrosion environment in above applications can also severely reduce the life of components as the low cycle fatigue, creep and thermal vibrations are the main causes of failure. From the literature review in Chapter 1, section 1.10, it is found that there were no reports published on LCF behaviour of Inconel 617 alloy under mixed salt environment. Hence the present investigation is aimed at studying the effect of oxidation without and with salt coating on LCF behaviour at 850^{o}C.

6.2 Methodology

Disc samples of 3 mm thickness and 10 mm diameter, and fatigue specimens with 5.5 mm gauge diameter and 15 mm gauge length (Fig. 2.2) were machined from annealed material of Inconel 617 alloy for static oxidation and hot corrosion studies. Both disc samples as well as fatigue samples were mechanically polished and then ultrasonic cleaning was carried out with acetone for 10 minutes. Samples were preheated at 150^{o}C in an oven for 8 hours to remove moisture. These preheated samples were kept in furnace at 850^{o}C for 50 h, 100 h, 250 h (100 x 2 cycles + 50 h), 500 h (100 h x 5 cycles) and 1000 h (100 h x 10 cycles) for oxidation.

For hot corrosion studies, both disc as well as fatigue samples were coated with supersaturated aqueous solution of 90%Na_2SO_4 + 10%NaCl salts. Then samples were kept in furnace for 50h, 100h, 250h (100 x 2 cycles + 50h), 500h (100h x 5 cycles) at 850^{o}C±5^{o}C. LCF tests were conducted under total strain controlled mode at 850^{o}C. All the tests were conducted at total strain amplitude ($\Delta\varepsilon_t/2$) of ±0.25%, at constant strain rate ($\dot{\varepsilon}$) of 5x10^{-3} s^{-1}. Detailed characterization was carried out using OM, TEM, SEM, XRD analysis and Electron Probe Micro Analysis (EPMA) for the fatigue tested samples.

6.3 LCF Behaviour

Table 6.1 shows the details of the LCF data of oxidized as well as salt coated and pre-exposed samples, tested at 850^{o}C at strain amplitude ($\Delta\varepsilon_t/2$) of ±0.25% and at strain rate ($\dot{\varepsilon}$) of 5x10^{-3} s^{-1}. It was found that oxidation up to 1000h did not show any significant effect on fatigue life, compared with that of the samples tested without oxidation (Chapter 5). Fatigue life of the samples with salt coating showed drastic reduction, with increase in the pre-exposure duration. The life was reduced almost by

40% compared with those of the samples without salt coating. The cyclic stress response (CSR) is the most important feature to describe the LCF behaviour and is used to predict the final stress level. Fig. 6.1a shows the CSR curves of the oxidized samples showing continuous cyclic hardening for all the samples. The rate of hardening was found to be similar for all the samples. Stress amplitude decreased with increase in the pre-exposure duration for the oxidized samples. Fig. 6.1b shows the cyclic stress response curves of the salt coated and pre-exposed samples depicting continuous cyclic hardening. There was continuous decrease in stress amplitude with increase in the duration of exposure. Cyclic stress amplitude of these samples was less than those of the oxidized samples without salt coating.

Table 6.1: Low Cycle Fatigue (LCF) Data of the Inconel 617 Alloy Tested at 850^{o}C at Strain Amplitude ($\Delta\varepsilon_t/2$) of ±0.25%, in Oxidized and Salt coated and Pre-exposed Condition at 850^{o}C for Different Durations.

Exposure duration, hours	N_f (Cycles)	$\Delta\varepsilon_p/2$	$\Delta\sigma/2$ (MPa)	σ_T (MPa)
Oxidation				
0	1190	0.00093	292	284
50	1275	0.00092	265	257
100	1201	0.00092	266	259
500	1256	0.00099	272	258
1000	1220	0.00089	244	230
Salt coating and Pre-exposure				
50	1045	0.00079	292	284
100	1098	0.00099	241	231
250	844	0.00097	256	240
500	653	0.00089	255	233

Fig. 6.2a and b shows the hysteresis loops at half-life cycle ($0.5N_f$) of the oxidized, and salt coated and pre-exposed samples respectively. These curves reveal decrease in stress amplitude with increase in the duration of the exposure. Table 6.1 presents different parameters derived from the hysteresis loops of half-life cycle ($0.5N_f$).

No significant change was observed in the values of plastic strain amplitude ($\Delta\varepsilon_p/2$) with increase in the duration of pre-exposure. Stress amplitude ($\Delta\sigma/2$) values may be seen to decrease with increase in the exposure duration. The tensile stress amplitude (σ_T) values were also given Table 6.1.

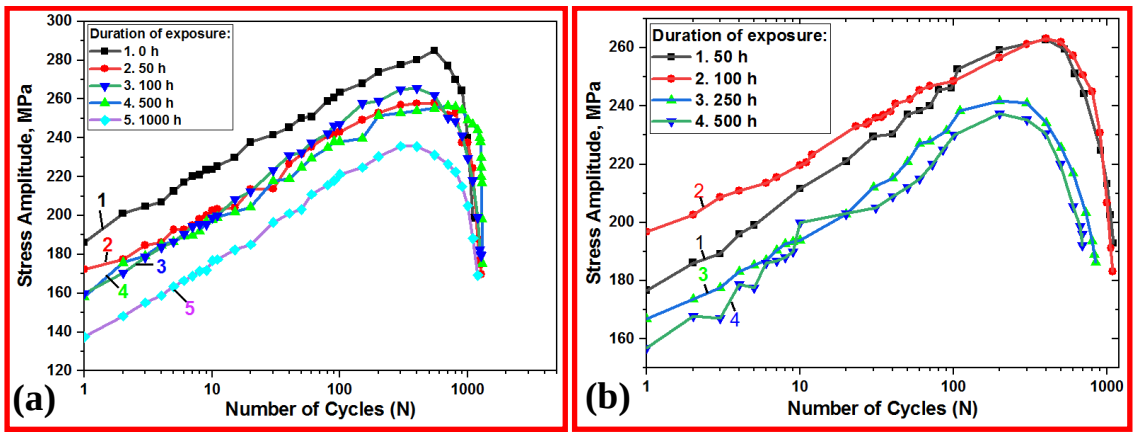

Fig. 6.1: Cyclic stress response curves during LCF testing at $\Delta\varepsilon_t/2 = \pm 0.25\%$ at 850°C (a) oxidized at 850°C and (b) salt coated and exposed in air at 850°C.

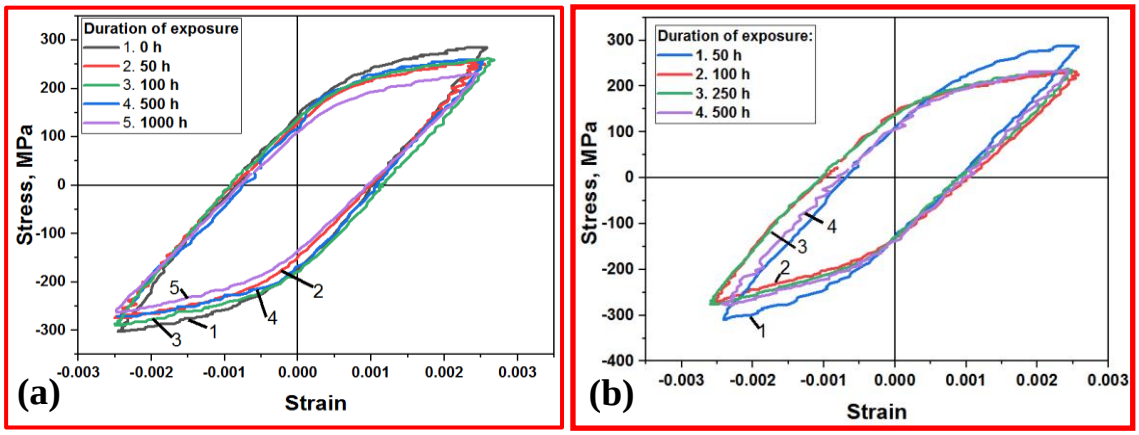

Fig. 6.2: Hysteresis loops of the half life cycle ($0.5N_f$) of different LCF samples tested at $\Delta\varepsilon_t/2 = \pm 0.25\%$ at 850°C: (a) oxidized at 850°C and (b) salt coated and pre-exposed in air at 850°C.

6.4 Deformation Behaviour

Fig. 6.3 shows bright field TEM micrographs of the fatigue specimen oxidized at 850°C in air for 50h and fatigue tested at 850°C and $\Delta\varepsilon_t/2 = \pm 0.25\%$. $M_{23}C_6$ carbides can be seen in the γ matrix as shown in Fig. 6.3a and dislocation tangles also can be

observed in Fig. 6.3b. The carbides formed during pre-oxidation for 50h were grown to larger size and additional carbides formed during LCF testing at 850°C were also observed as indicated in Fig. 6.3c. Fig. 6.4 shows the HAADF-STEM, EDX elemental mapping of the bigger carbide particle as shown in Fig. 6.3c, confirming the presence of both chromium and molybdenum in the carbide particles. These carbides were confirmed as $M_{23}C_6$ type of carbides as given in Chapter 5. The carbides formed during the pre-exposure of 50 h were bigger in size and the additional carbides formed during deformation are smaller in size. Fig. 6.5a shows carbides in the γ matrix of the specimen oxidized for 500 h. Fig. 6.5b shows dislocation tangles formed. No change was observed in dislocation density of the specimen. Fig. 6.5c shows the carbides formed during oxidation for 500 h were grown to larger size compared to the size of the carbides in 50 h sample.

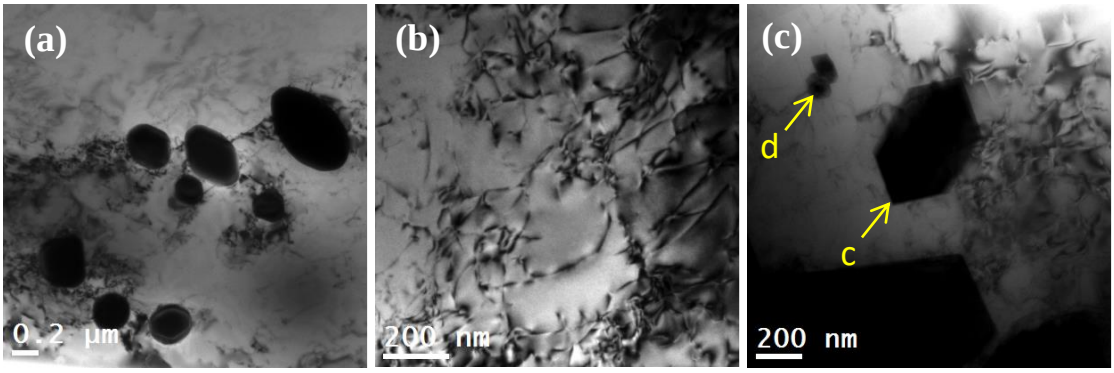

Fig. 6.3: TEM micrographs of the LCF samples, oxidized at 850°C for 50h and tested at $\Delta\varepsilon_t/2 = \pm 0.25\%$ at 850°C, showing: (a) $M_{23}C_6$ carbides in the γ matrix (b) dislocation tangles and (c) carbides formed during oxidation (indicated by 'c') and formed during deformation in LCF testing (indicated by 'd').

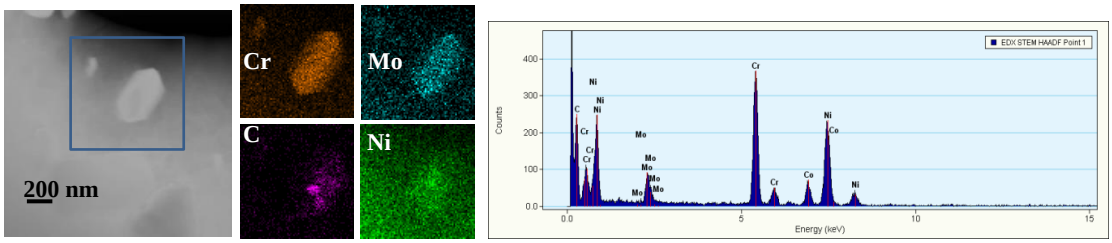

Fig. 6.4: HAADF-STEM, EDX elemental mapping of the carbides shown in Fig. 6.3c, confirming the presence of Cr, Mo in the carbide.

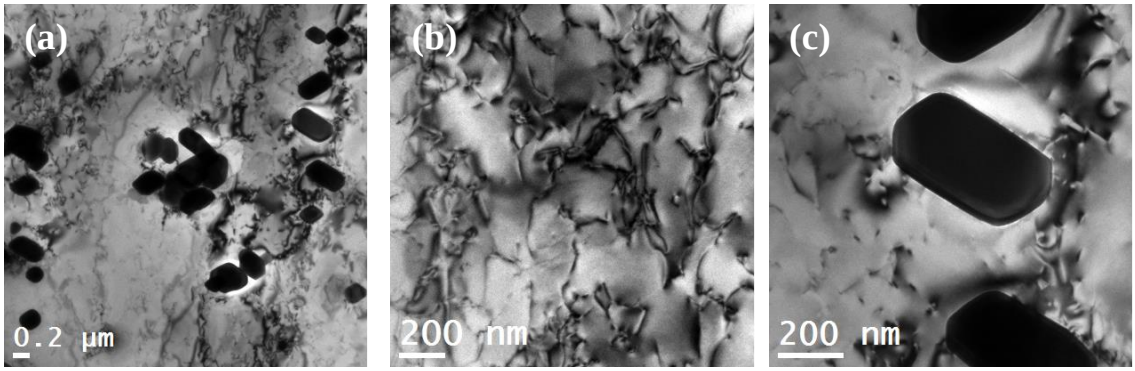

Fig. 6.5: TEM micrographs of the LCF samples, oxidized at 850°C for 500h and tested at $\Delta\varepsilon_t/2 = \pm 0.25\%$ at 850°C, showing: (a) $M_{23}C_6$ carbides in the γ matrix, more in number than those in 50h exposed sample (b) dislocation tangles and (c) carbide formed during oxidation.

Figs. 6.6 and 6.7 show TEM micrographs of the LCF tested samples salt coated and pre-exposed for 50h and 500h respectively. The carbides in the sample exposed for 50 h are similar in size and number to those observed in the tested sample oxidized for the same duration. The 500 h sample had very less number of carbides compared to those in other samples. Dislocation density was found to be also same for samples subjected to 500 h exposure. More elongated carbides were formed which were bigger in size in sample exposed to 500h compared to those observed in the samples exposed to 50 h of duration.

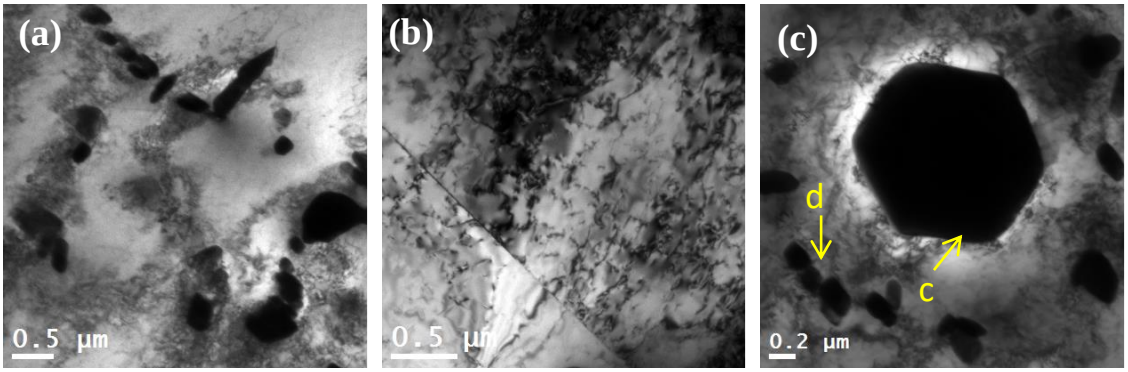

Fig. 6.6: TEM micrographs of the LCF samples, salt coated and exposed at 850°C for 50h, tested at $\Delta\varepsilon_t/2 = \pm 0.25\%$ at 850°C, showing: (a) $M_{23}C_6$ carbides in the γ matrix, more in number than those in the sample oxidized for 50h, (b) dislocation tangles and sub grain formation and (c) carbides formed during pre-exposure (indicated as 'c') and formed during deformation in LCF testing (indicated as 'd').

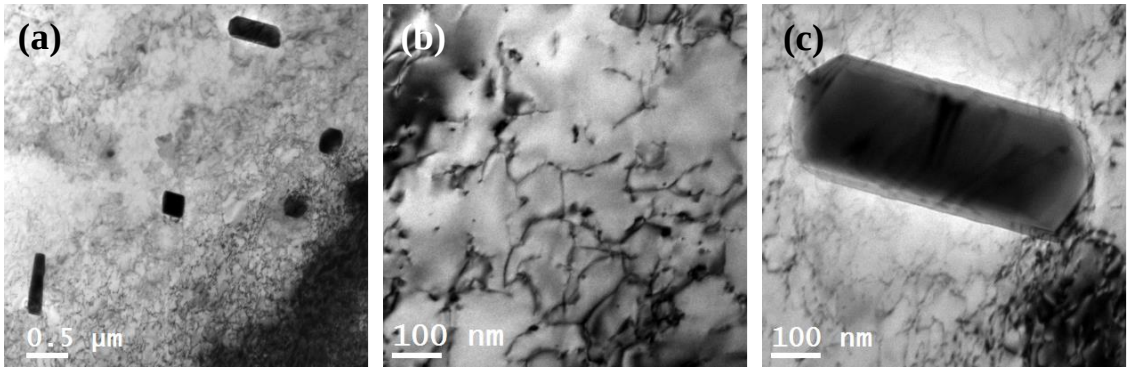

Fig. 6.7: TEM micrographs of the LCF samples, salt coated and exposed at 850^{o}C for 500h, tested at $\Delta\varepsilon_t/2 = \pm 0.25\%$ at 850^{o}C, showing (a) $M_{23}C_6$ carbides in the γ matrix (b) dislocation tangles and (c) carbides formed during pre-exposure.

6.5 Fracture Behaviour

Fig. 6.8 shows fracture surfaces of the LCF tested samples, oxidized for 50h and 500h. Arrows indicate the multiple locations of crack initiation on surface, in both the cases, though the number of initiation sites was found to be more in the 500h oxidized sample. Crack nucleation occurred by surface ridging (Fig. 6.8). Ratchet lines at different heights in different directions (Figs. 6.8a and c) can be seen in both the conditions. Inter-striation spacing was found to be 1-2 μm and no difference was observed in inter-striation spacing in both the conditions.

Figs. 6.9 and 6.10 show fracture surfaces of the salt coated samples pre-exposed for 50h and 500h respectively, showing multiple crack initiation sites. The hot corroded area is clearly visible as a layer as shown by arrow in Fig. 6.9b and 6.10b. The thickness of the layer was increased for the 500h sample. The crack initiation sites were observed in the subsurface (Fig. 6.10b). Inter-striation spacing was found to be 1-2 μm, similar to that of oxidized samples without coating, in both the conditions.

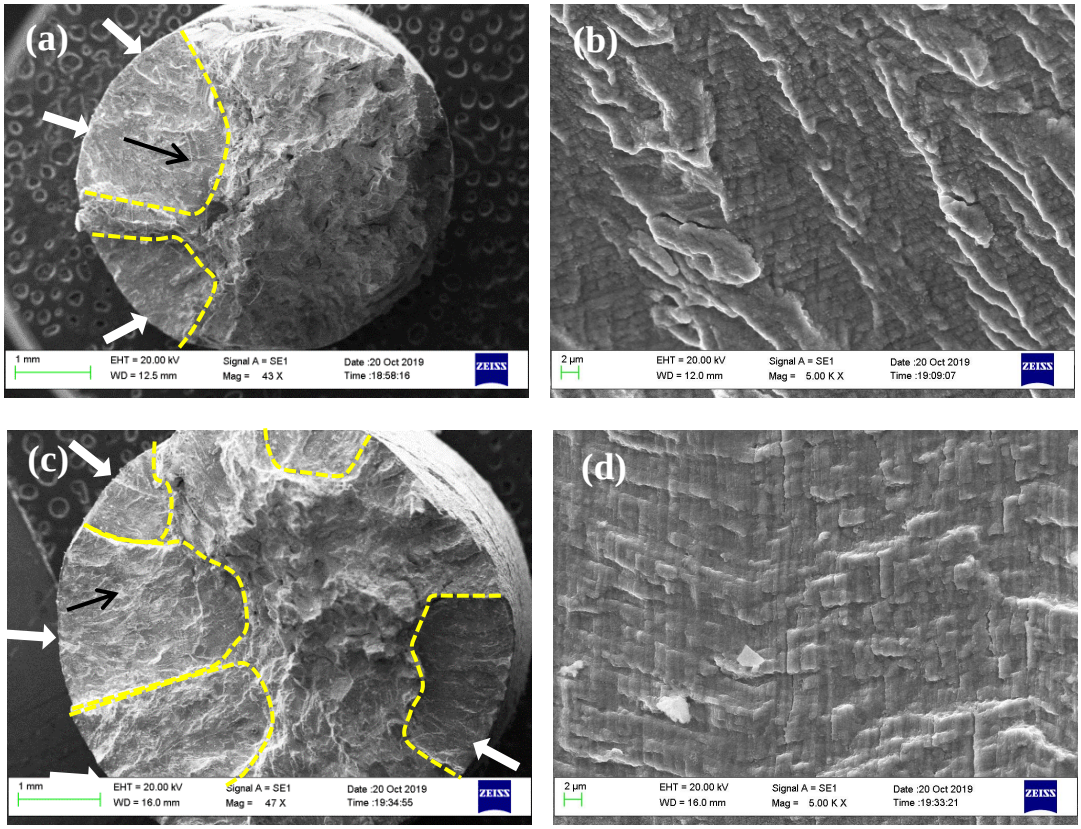

Fig. 6.8: SEM fractographs of the LCF samples, tested at 850^{o}C and at $\Delta\varepsilon_t/2 = \pm 0.25\%$. Samples oxidized at 850^{o}C for 50h showing (a) multiple crack initiation site (white arrow), fatigue crack growth direction (dark arrow) (b) Striation morphology. Samples oxidized at 850^{o}C for 500h showing (c) multiple crack initiation site (white arrow), fatigue crack growth direction (dark arrow) (d) Striation morphology.

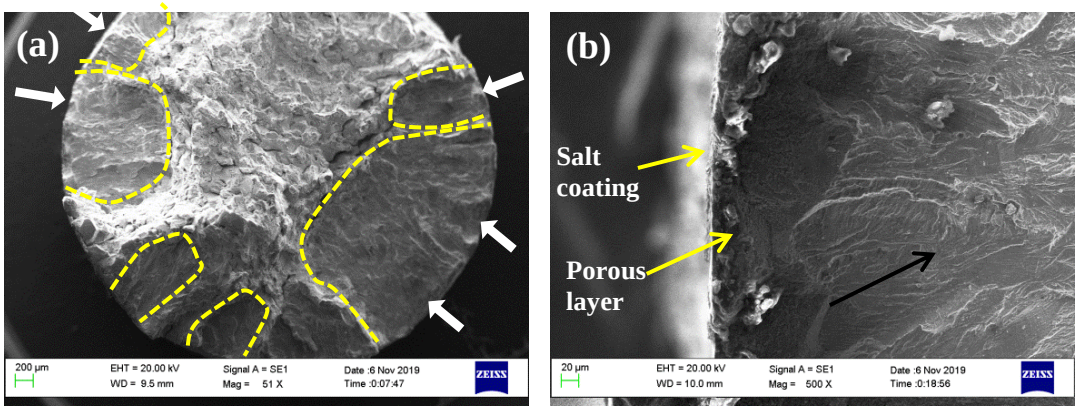

Fig. 6.9: SEM fractographs of the LCF samples, salt coated and pre-exposed at 850^{o}C for 50h and tested at at 850^{o}C and at $\Delta\varepsilon_t/2 = \pm 0.25\%$, showing: (a) multiple crack initiation sites (indicated by white arrow) and (b) fatigue crack growth direction (indicated by black arrow).

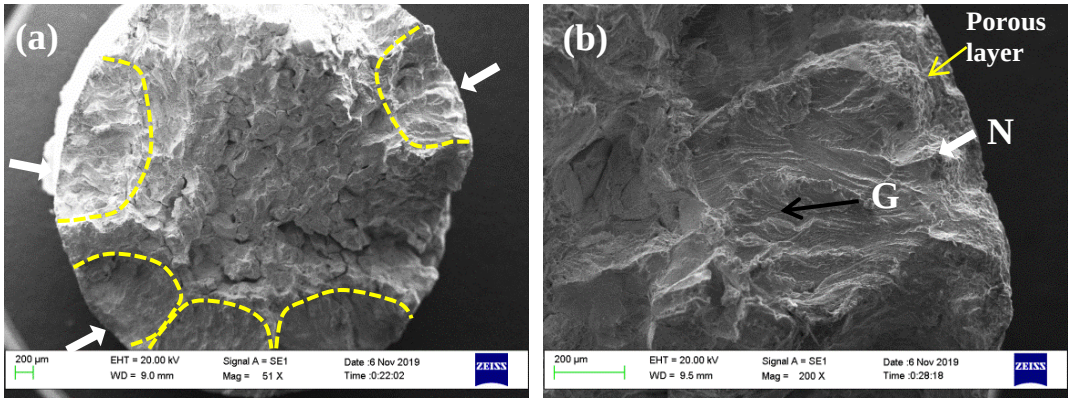

Fig. 6.10: SEM fractographs of the LCF samples, salt coated and pre-exposed at 850^{o}C for 500 h and tested at 850^{o}C and at $\Delta\varepsilon_t/2 = \pm$ 0.25%, showing (a) multiple crack initiation sites (indicated by white arrow) and (b) fatigue crack growth direction (indicated by 'G'). Crack initiation site indicated by 'N'.

Fig. 6.11a shows optical micrograph of the longitudinal sectioned surfaces of the 50 h salt coated and pre-exposed fatigue tested sample. Primary crack growth was initially intergranular and later transformed to transgranular. All the multiple cracks were intergranular at the surface and the intergranular cracks propagated up to a depth of ≃40-50µm. Fig. 6.11b shows optical micrographs of longitudinal sectioned surfaces of the salt coated and 500 h exposed, fatigue tested samples. Primary crack propagation was mainly of intergranular nature and changed into transgranular one progressively. The depth of the porous surface layer on the 500 h exposed samples (≃100-120 µm) was more compared with that in sample exposed for 50 h.

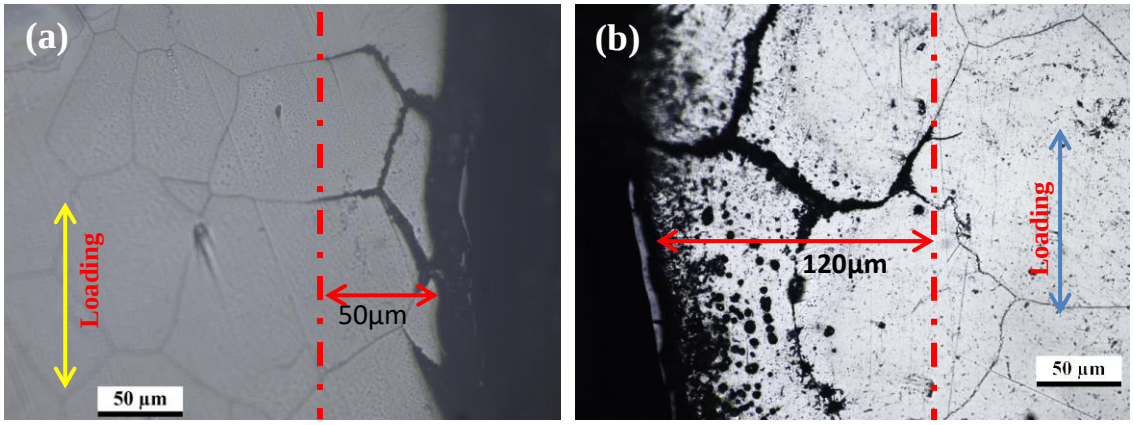

Fig. 6.11: Optical micrographs of longitudinal cross section of the fractured LCF specimen, salt coated and pre-exposed at 850°C, tested at 850°C, $\Delta\varepsilon_t/2 = \pm 0.25\%$ (a) 50 h sample showing intergranular cracking and depth of the region of intergranular cracking is ≃ 40-50µm (b) 500 h sample showing wide intergranular cracks and porous corroded layer. Depth of the region of intergranular cracking is ≃100-120 µm.

6.6 Oxidation and Hot Corrosion Behaviour

Fig. 6.12 shows the digital photographs of the disc samples exposed to oxidatin for various durations at 850°C, clearly shows the change in the shiny surface to gray colour on exposing at high temperaure for 50 h. The colour of the surface changed to dark gray with increase in the duration. The colour of the samples changed to black for the samples exposed to 1000 h duration. Pitting was not observed on the surface and there was no evidence of peeling of oxide layer which indicate there was no formation of thick oxide scales.

Fig. 6.12: Digital photographs of the disc samples exposed to oxidation at 850°C for various durations: (a) as polished (b) 50 h (c) 100 h (d) 500 h and (e) 1000 h.

Fig. 6.13 shows the digital photographs of the salt coated samples and pre-exposed for vairous durations at 850^{o}C. The salt coating changed to greenish colour on the surface with increase in the duration of exposure. The salts observed to be melted on the surface at this temperature and appearance of the partial surface changed to greenish colour for the 50 h exposed samples. The surface turned to be complete greenish colour for 250 h and 500 h samples. And also the thickness of the layer also was found to be increased with duration of pre-exposure. The salt products started to peel off after changing to greenish colour and with increase in duration. The reaction of the salts with oxygen in the air at the elevated temperature contributed to the formation of porous layer of oxides. The photograph for 500 h pre-exposed sample (Fig.6.13 e) shows the surface after peeling off of salt products where pitting can be clearly observed on the surface.

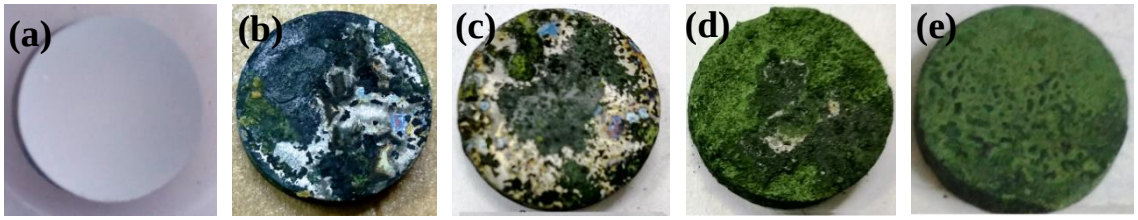

Fig. 6.13: Digital photographs of the disc samples salt coated and pre-exposed at 850^{o}C for various durations: (a) as coated (b) 50 h (c) 100 h (d) 250 h and (e) 500 h.

Fig. 6.14 shows the plot of weight change or gain against exposure duration (hours) for both samples exposed with salt coating and without salt coating. It can be observed from the plot that weight gain occurred for both the conditions of the samples. Rapid weight change can be noticed with increase in the exposure duration up to 100 h, after that weight increase observed depicted slower rate. The weight gain for samples with salt coating was more compared to that of the mere oxidised samples which was almost two times. Formation of oxides of substrate elements has contributed for

increase in the weight gain in both the cases. The results are in agreement with the observation of several researchers [68, 69, 137].

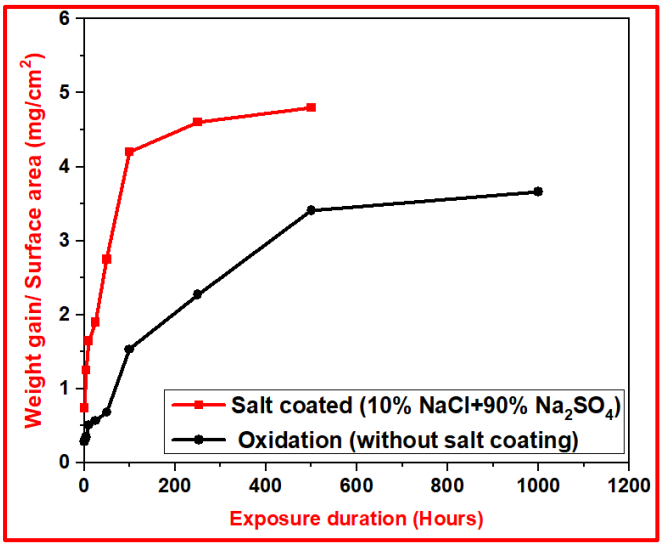

Fig. 6.14: Plot of weight change with respect to duration of exposure (hours) for the samples of Inconel 617 alloy with salt coating and without salt coating.

Fig. 6.15a shows X-Ray diffraction data of the disc samples (static) oxidized for 50 h and 500 h. The X-Ray peaks of the sample without exposure is also shown in Fig. 6.15a for comparison, which contains reflections of γ matrix of the Inconel 617 alloy. The oxidized samples show Cr_2O_3, $NiCr_2O_4$ and NiO along with matrix reflections indicating formation of different oxides in the 50 h oxidized sample. Similar results were obtained also for the 500 h oxidized samples except the increase in the number of peaks representing TiO_2. Fig. 6.15b shows X-Ray diffraction data of the disc samples (static) salt coated and oxidized for 50 h and 500 h. In addition to the oxide products observed above for oxidized samples, sulphide product of CrS was found for the samples with salt coating. The oxide products observed are in agreement with the results obtained by the previous researchers [68, 69, 137-141].

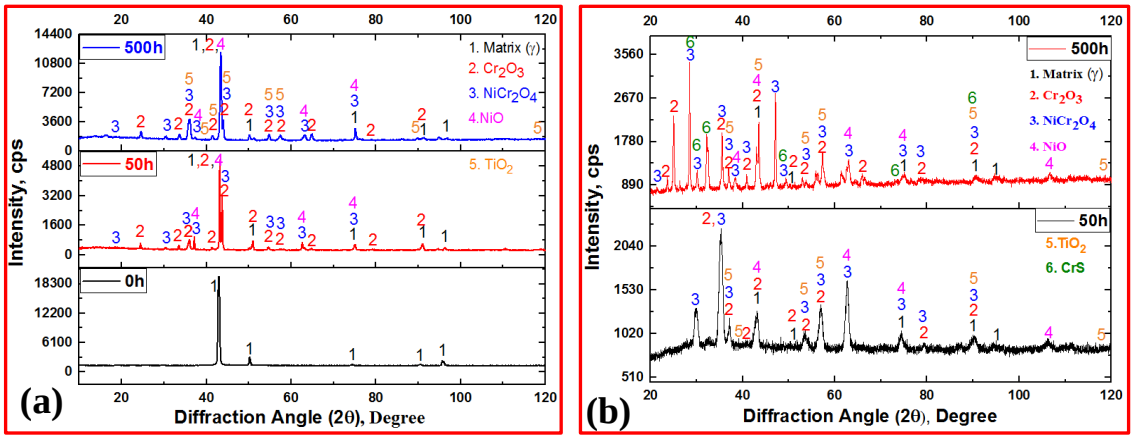

Fig. 6.15: XRD analysis of the disc samples (a) un-oxidized and those oxidized in air at 850^{o}C for 50 h and 500 h (b) salt coated and pre-exposed in air at 850^{o}C for 50 h and 500 h.

Fig. 6.16 shows SEM micrographs of cross sections of the fatigue tested samples, oxidized for 50 h and 500 h. Depth of the porous oxidized layer was found to be increased with increase in the duration of oxidation. Depth of the porous layer was 8-10 μm for the 50 h oxidized sample (Fig. 6.16a) and 15-20 μm for the 500 h oxidized sample (Fig. 6.16b). The size of voids was also increased and these voids were merged at some places which resulted in increase in the size. The porous surface layer was not visible in the bare sample, which was fatigue tested without any exposure (Inset image in Fig. 6.16a).

Fig. 6.17 shows cross sections of the salt coated fatigue samples pre-exposed for 50 h and 500 h, and tested at 850^{o}C. Increase in the depth of hot corroded layer with increase in duration of exposure can be clearly seen. The depth of corroded porous layer was 10-15 μm for 50 h samples whereas the layer was increased to 40-50 μm in the 500 h sample. The cracks as well as spinels, can also be seen clearly in this case. The number and intensity of the cracks were increased with increase in the exposure duration i.e. for 500 h pre-exposed sample compared to those in 50 h pre-exposed sample.

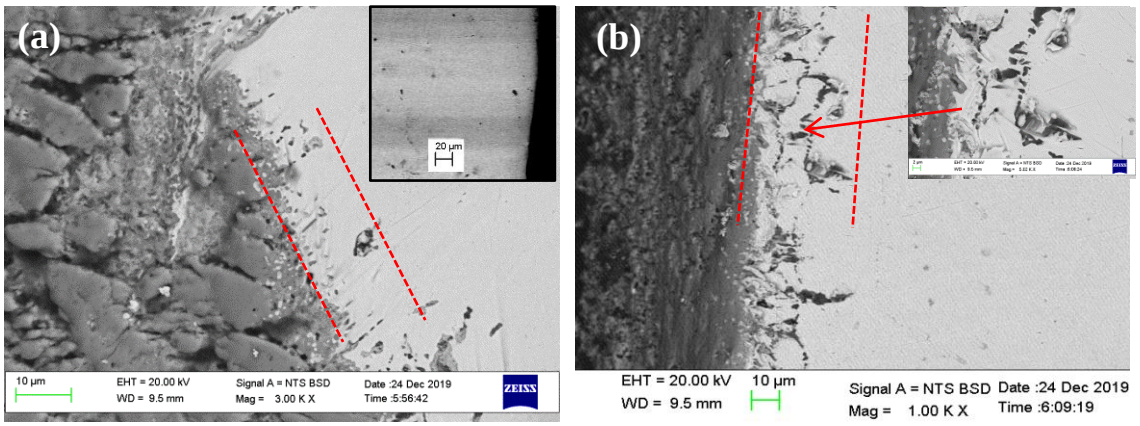

Fig. 6.16: SEM micrographs of longitudinal cross section of fractured LCF specimens, tested at 850°C and at $\Delta\varepsilon_t/2 = \pm 0.25\%$ (a) oxidized at 850°C for 50 h showing depth of the porous oxidized layer (≃8-10 µm). Inset image shows cross section of the sample tested without any pre-exposure. (b) Oxidized at 850°C for 500h showing depth of porous oxidized layer (≃15-20 µm) and void formation.

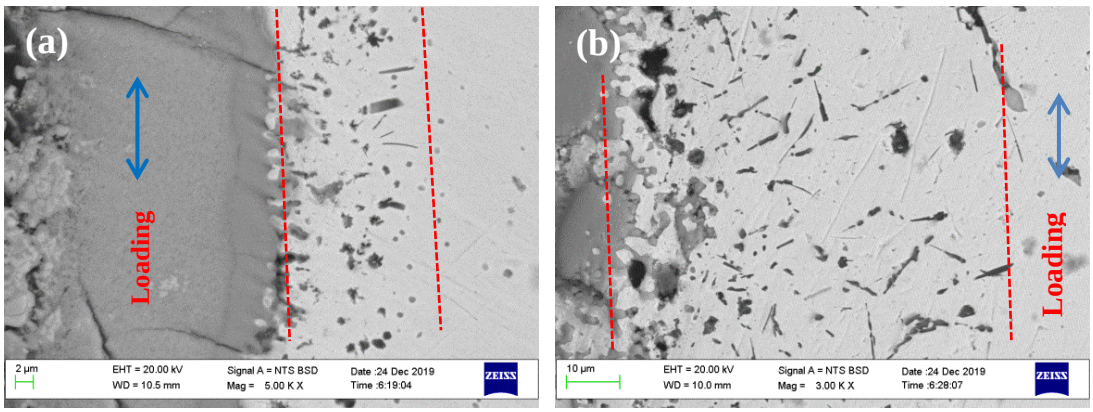

Fig. 6.17: SEM micrographs of the longitudinal section of fractured LCF specimens, tested at 850°C and at $\Delta\varepsilon_t/2 = \pm 0.25\%$ showing magnified view of the surface region affected by hot corrosion (porous layer) for (a) salt coated and pre exposed at 850°C for 50 h, depth of the porous oxidized layer is 10-15 µm (b) salt coated and pre exposed at 850°C for 500 h, depth of the porous oxidized layer is≃ 40-50 µm.

Fig. 6.18 shows EMPA elemental mapping details of the 50 h and 500 h oxidized fatigue samples, tested at 850°C. Fig.6.18a indicates the external surface oxide layer as Cr_2O_3 below which the Cr depletion layer (5-8 µm) was observed. Internal oxide of Al_2O_3 layer was formed up to the depth of 8-10 µm. For the 500 h oxidized sample (Fig. 6.18b) the oxide layers are same except the formation of TiO_2 as an external layer in the same position as Cr_2O_3 layer. The thickness of both the external

and internal oxide layers was increased, with increase in the duration. Al_2O_3 oxide layer was formed especially along the voids or spinels. Table 6.2 shows the thickness of the Cr depletion and Al_2O_3 internal oxide layer for the oxidized and salt coated and pre-exposed samples.

Table 6.2: Thickness of the Cr Depletion Layer and Al_2O_3 Internal Oxide Layer.

Sample	Cr depletion layer, µm	Al_2O_3 internal oxide layer, µm
Oxidized for 50 h	5-8	8-10
Oxidized for 500 h	35-40	35-40
Salt coated and Pre-exposed for 50 h	15-18	15-20
Salt coated and Pre-exposed for 500 h	65-70	70-80

Fig. 6.19 shows EPMA elemental mapping details for the fatigue tested samples of salt coated and pre-exposed for 50 h and 500 h. Fig. 6.19a shows that surface oxide layer of $NiCr_2O_4$ formed above Cr_2O_3 layer. The Cr depleted region with thickness of 15-20 µm was found beneath the Cr_2O_3 surface oxide layer. The Al_2O_3 layer was observed in the same region of Cr depleted layer but not as continuous layer rather as discontinuous thin oxides containing voids. Sulphur ingression was observed though to minimal area. The thickness of oxide layers was increased with increase in duration of exposure as shown in Fig. 6.19b. The sulphur ingression along grain boundaries was observed where the intergranular hot corrosion has occurred. The sulphur product is primarily Chromium sulphide (CrS) as evidenced by presence of Cr and S in the same region of the cracks as shown by arrows in Fig. 6.19b.

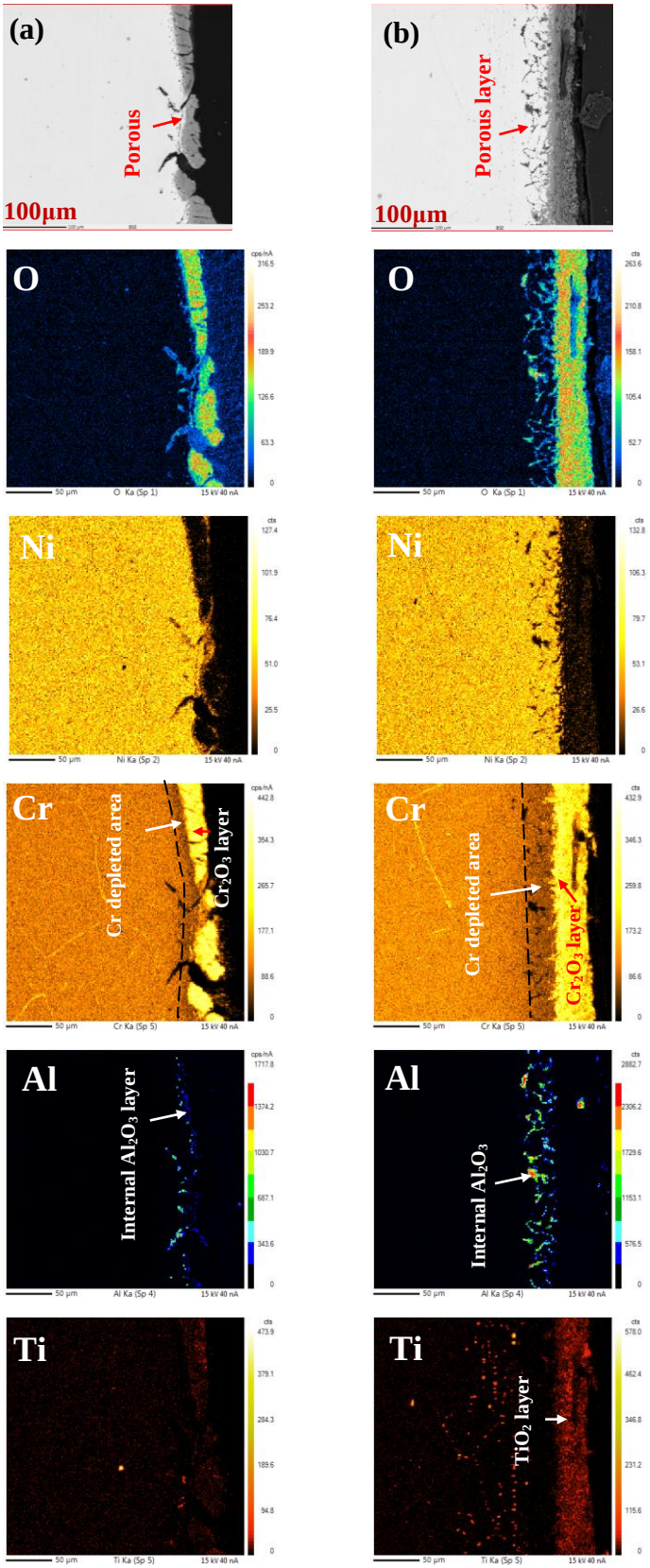

Fig. 6.18: BSE images of the cross sectional surfaces and EPMA elemental mapping of the LCF sample oxidized in air at 850°C and tested at $\Delta\varepsilon_t/2 = \pm 0.25\%$ at 850°C, showing the effect of duration of exposure in air for: (a) 50 h and (b) 500 h.

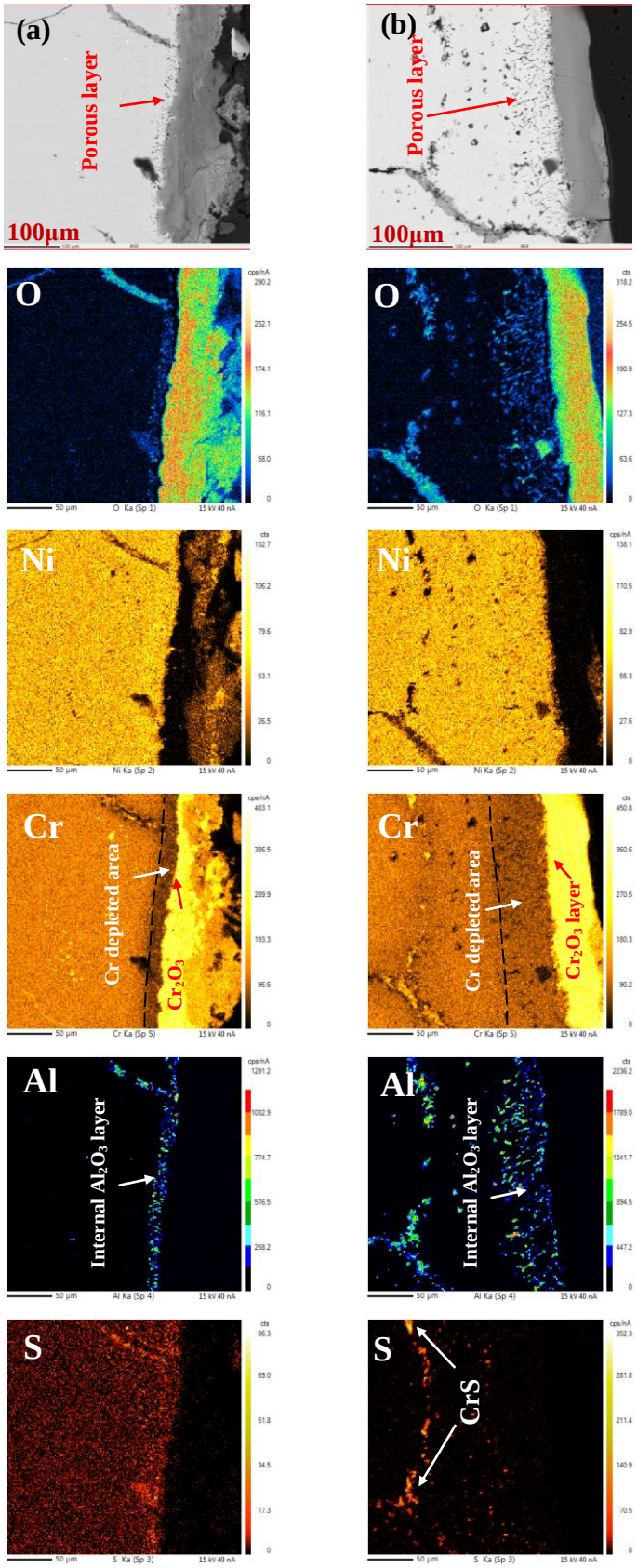

Fig. 6.19: BSE images of cross sectional surfaces and EPMA elemental mapping of the LCF specimens salt coated and pre-exposed in air at 850^{o}C, tested at 850^{o}C and at $\Delta\varepsilon_t/2 = \pm 0.25\%$, showing the effect of duration of exposure in air for: (a) 50 h and (b) 500 h.

6.7 Discussion

6.7.1 LCF Behaviour

Fatigue life of a material depends on the applied stress/strain amplitude, strain rate, temperature and the environment. In the present case, all the other parameters were kept constant except environment, to determine the effect of pre-exposure without and with salt coating on fatigue behaviour. The samples that were subjected to oxidation without salt coating did not exhibit any effect on fatigue life. The influence of hot corrosion in the pre-exposed salt coated samples was more severe and showed drastic reduction in life due to sulphide ingression into the substrate material and caused intergranular corrosion. The sulphide ingression was more in the 500h exposed samples compared with that of the 50h exposed sample, which reduced the fatigue life drastically by 40%. The observed reduction in the cyclic stress amplitude can be attributed to reduction in cross sectional area due to formation of scale and voids in the surface region. The reduction in cross sectional area was increased with increase in the duration due to increase in the thickness of the oxidized layer as evidenced by the metallographic examination [142].

6.7.2 Deformation Behaviour

Fig. 6.20a shows TEM micrograph of the disc sample oxidized at 850^{o}C for 500h. Formation of carbide precipitates which are round in shape and few in numbers can be seen after oxidation. Slightly larger sized precipitates were formed during oxidation. TEM micrograph in Fig. 6.20b shows the precipitates formed during LCF testing of the sample at ε_t = ±0.25% and 850^{o}C, without any pre-exposure. The precipitates formed during deformation due to cyclic straining were irregular in shape. The precipitates that were formed during aging were deformed and changed their shape

from round to different shapes as shown in Fig. 6.20b. Precipitation of less number of carbides during deformation of the oxidized samples could be due to less carbon available for further carbide formation as already carbides were formed during exposure. More number of carbides and coarser carbides were formed in the 500h exposed samples due to extended duration of oxidation at 850^{o}C and also due to growth of already formed precipitates. But during testing, because of same test conditions, the carbide formation and dislocation substructure were similar. There was no difference in the observed deformation behaviour because the strain amplitude and temperature remained same for both the samples.

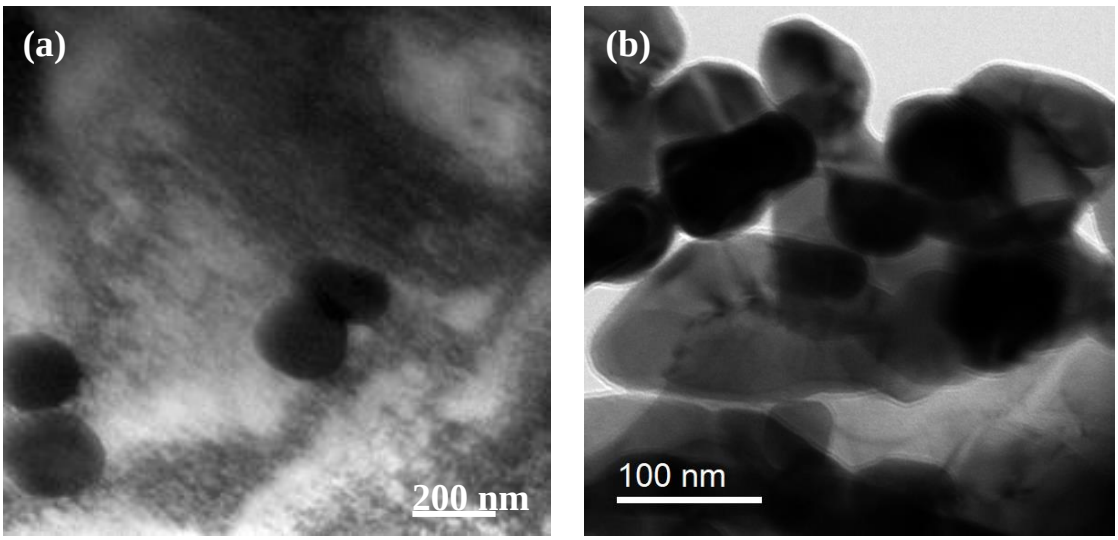

Fig. 6.20: TEM micrographs showing (a) carbides formed in the disc sample oxidized at 850^{o}C and (b) carbides formed in the fatigue sample without any pre-exposure, tested at 850^{o}C, $\Delta\varepsilon_t/2 = \pm 0.25\%$.

From the studies mentioned in Chapter 5 and from the earlier literature on the Inconel 617 alloy, it can be observed that mainly two major phases namely, carbides and γ' [$Ni_3(Ti,Al)$] form in the γ matrix during high temperature exposure [12, 13]. From the study of Ni-Cr-Al and Ni-Cr-Ti ternary systems at 850^{o}C [140, 143-145] and as discussed in Chapter 5, it can be inferred that γ' does not exist for nominal

composition of Inconel 617 alloy at 850^{o}C. The experimental results observed in the present investigation using STEM-HAADF analysis and TEM micrographs are in good aggreement with the stability of the phases reported.

6.7.3 Fracture Behaviour

Fatigue failure occurs mainly by crack initiation and crack propagation. The number of cracks that initiate generally from a free surface may be one or more depending on the temperature, strain rate, and environment. The cracks that are initiated propagate in three stages, stage I (propagation of the initiated crack along shear direction), stage II (growth perpendicular to applied stress and depends on material) and Stage III (tensile over load fracture by formation of voids and growth). As the temperature of present investigation was high (850^{o}C), multiple crack initiation was observed (Fig. 6.8- Fig. 6.10). In the case of salt coated samples tested under LCF, damage of the protective Cr_2O_3 layer due to salts in general, chloride ions in particular, may not be effective due to synergetic effect of cyclic loading. In these samples, wedge shaped crack nucleation occurred in the areas of sulphides due to sulphidation reaction and oxide inclusions at some grain boundaries on the substrate metal. This generally occur perpendicular to loading axis and below the strong oxide layers (Fig. 6.9 & 6.10). Fig. 6.10 clearly shows the crack initiation sites just after the oxide layers. These cracks propagated uninterruptedly causing failure of the sample. The initial intergranular crack propagation mode remained till the depth of the corroded layer and later on changed into transgranular one. Oxide particles or salt products which were observed on fracture surfaces migrated inside the surface during fatigue testing and caused crack propagation to continue in those directions. From the studies of Ni-Cr-Al ternary systems[140, 144,145], it can be inferred that Inconel 617 alloy, which contains high Cr >15 wt.% and low Al < 2 wt.% content, forms an external layer of Cr_2O_3 and the internal layer of

Al_2O_3 due to oxidation of Al. It is also reported by Christ et al. [146] that the Co and Mo have no significant role in the oxidation of Inconel 617 alloy. The results of the present investigation are in line with these observations.

6.7.4 Oxidation and Hot Corrosion Behaviour

Oxidation of the Inconel 617 takes place by movement of chromium ions through the thick Cr_2O_3 layer. Oxygen reacts with Cr at surface scale/interface. Titanium oxide was also formed additionally in the Cr_2O_3 scale layer in the 500h oxidized sample. Previous researchers [68, 140, 141] reported formation of oxide layers of $NiO/NiCr_2O_4/Cr_2O_3$ at 900^{o}C after 1000h but in the present investigation, presence of these oxides was confirmed by XRD analysis after exposing the alloy at 850^{o}C for 50h. Oxygen diffuses inward whereas the metal ions of Cr and Ti diffuse outward from the substrate to promote continuous growth of these oxides scale and porous layer [145, 147, 148]. Due to low concentration of Titanium in this alloy, formation of Cr oxide was dominant compared to the formation of TiO_2.The oxidation reactions are as follows:

$Ni + 1/2O_2 \rightarrow 2NiO$ ---------- (6.1)

$2Cr + 3/2O_2 \rightarrow Cr_2O_3$ ---------- (6.2)

$NiO + Cr_2O_3 \rightarrow NiCr_2O_4$ ---------- (6.3)

$Al + 3/2O_2 \rightarrow Al_2O_3$ ---------- (6.4)

$2Ti + O_2 \rightarrow 2TiO_2$ ---------- (6.5)

Longer durations are required for Na_2SO_4 to come in contact with the substrate if no other salt is available. However, the presence of NaCl continuously destroys the strong oxide layers that are formed and exposes the substrate to come in contact with Na_2SO_4. Cl^- ions formed by chlorination with metallic elements quickly penetrate

through fluxing voids and also pass through the grain boundaries and form chromium chloride, which is volatile in nature [149]. The chlorination reactions are as follows:

$NaCl \rightarrow Na^{+} + Cl^{-}$ ---------- (6.6)

$Cr + Cl_2(g) \rightarrow CrCl_2$ ---------- (6.7)

$Ti + 2Cl_2(g) \rightarrow TiCl_4$ ---------- (6.8)

$Al^{3+} + 3Cl^{-}(g) \rightarrow AlCl$ ---------- (6.9)

These products diffuse to surface in the same path as that of Cl^{-} ions. These chlorides re-oxidize and form Cl_2 again cyclically and cause uninterrupted corrosion by penetrating again into the metal. Diffusion of sodium was not observed in the base metal. Neither sodium nor chorine products were noticed in the XRD analysis or EPMA analysis. However, the dissolution of $NaCl/Na_2O$ in Cr_2O_3 forms $Na_2Cr_2O_7$ which evaporates during the process. These reactions are as follows:

$2NaCl + Cr_2O_3 + 2O_2 \rightarrow Na_2Cr_2O_7 + Cl_2(g)$ ---------- (6.10)

$Na_2O + Cr_2O_3 + 3/2O_2 \rightarrow Na_2Cr_2O_7(g)$ ---------- (6.11)

Na_2SO_4 promotes sulphidation at grain boundaries in the inner surface of material which contributes to intergranular hot corrosion. This grain boundary cracking resulted in increased stress in that region and led to premature failure. From the EPMA elemental mapping analysis (Fig. 6.19b), it is clearly evident that sulphur was present along with chromium (as shown by arrows) along the cracks and absence of Ni in the same regions. This confirms that the CrS as the sulphide product which was detrimental and caused drastic reduction in fatigue life. These reactions are as follows:

$Na_2SO_4 \rightarrow Na^{+} + SO_4^{2-}$ ---------- (6.12)

$SO_4^{2-} \rightarrow S^{2-} + 2O_2$ ---------- (6.13)

$Cr + S^{2-} \rightarrow CrS$ ---------- (6.14)

The synergistic effect of NaCl and Na_2SO_4 caused severe hot corrosion, hence during cyclic loading, this alloy suffered drastic reduction in fatigue life. Figs. 6.21 and 6.22 show schematic diagrams to depict the mechanisms of process of oxidation and fracture from LCF discussed above for oxidized and hot corroded samples respectively.

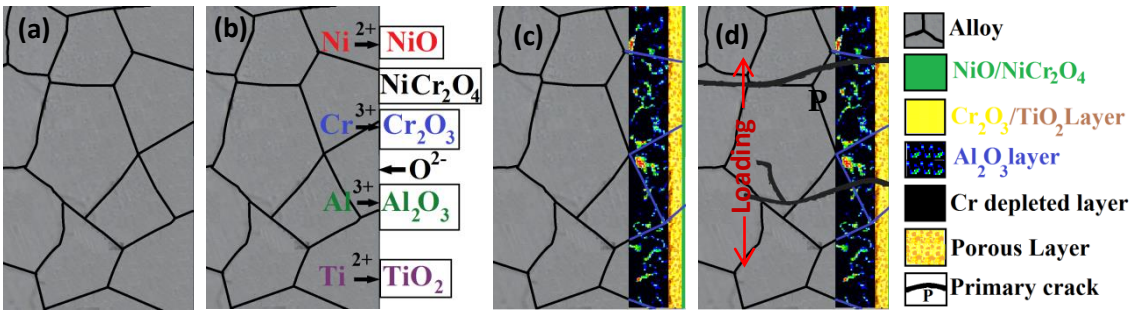

Fig. 6.21: Schematic representation of the process of oxidation and fracture from LCF showing: (a) initial microstructure (b) oxidation at 850°C (c) oxidized surface region and (d) failure due to LCF at 850°C and at $\Delta\varepsilon_t/2 = \pm 0.25\%$.

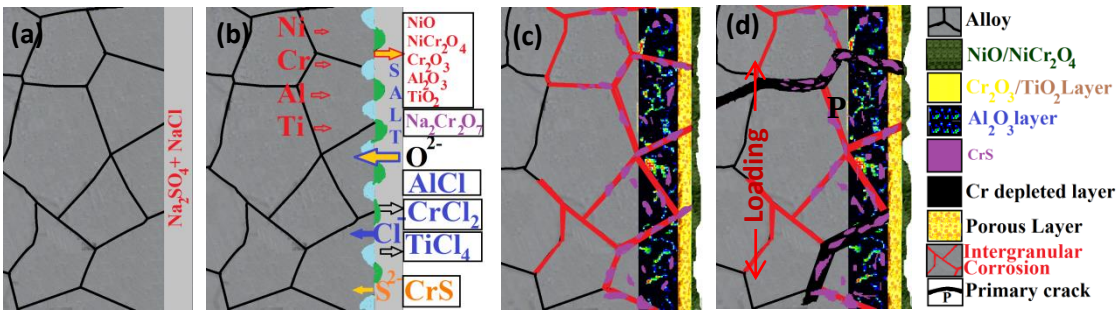

Fig. 6.22: Schematic representation of the process of hot corrosion and fracture from LCF showing: (a) initial microstructure and salt coating (b) hot corrosion during exposure at 850°C (c) damage from hot corrosion and (d) failure of hot corroded sample from LCF at 850°C and at $\Delta\varepsilon_t/2 = \pm 0.25\%$.

6.8 Chapter Summary

The following conclusions can be drawn from the present chapter.

1. Duration of pre-exposure to oxidation up to 1000 hours did not have significant effect on fatigue life of the Inconel 617 alloy. The stress amplitude decreased with increase in the duration of oxidation due to increase in the depth of porous

layer from oxidation. Strong surface oxide layer of Cr_2O_3 and inner oxide layer of Al_2O_3 were formed in the same vicinity of Cr depletion region.

2. The fatigue life of the salt coated and pre-exposed samples was reduced drastically with increase in the duration of pre-exposure up to 500h. Stress amplitude was reduced with increase in the duration of pre-exposure due to increase in the thickness of the hot corroded layer and consequent reduction in cross sectional area of the specimen.
3. Fatigue crack initiation occurred from the surface for the oxidation samples whereas it was from the subsurface for the salt coated and pre-exposed samples. The crack propagation was intergranular and progressively transformed to transgranular mode.
4. Deformation behaviour was similar for the both oxidized as well as salt coated and pre-exposed samples except the evidence of increase in the number of precipitates with increase in the duration of pre-exposure. The precipitates formed during deformation were smaller in size than the precipitates formed during pre-exposure.
5. Ingression of sulphur into base metal caused the formation of chromium sulphide (CrS) which reduced the fatigue life drastically. Crack propagation occurred along the intergranular corrosion layer and the depth of this layer increased with increase in the duration of oxidation.